Second-Order Topological Phases in Non-Hermitian Systems

Tao Liu,[1,*] Yu-Ran Zhang,[1,2] Qing Ai,[1,3] Zongping Gong,[4,†] Kohei Kawabata,[4,‡] Masahito Ueda,[4,5,§] and Franco Nori[1,6,‖]

[1]*Theoretical Quantum Physics Laboratory, RIKEN Cluster for Pioneering Research, Wako-shi, Saitama 351-0198, Japan*
[2]*Beijing Computational Science Research Center, Beijing 100193, China*
[3]*Department of Physics, Applied Optics Beijing Area Major Laboratory, Beijing Normal University, Beijing 100875, China*
[4]*Department of Physics, University of Tokyo, 7-3-1 Hongo, Bunkyo-ku, Tokyo 113-0033, Japan*
[5]*RIKEN Center for Emergent Matter Science (CEMS), Wako, Saitama 351-0198, Japan*
[6]*Department of Physics, University of Michigan, Ann Arbor, Michigan 48109-1040, USA*

(Received 9 October 2018; published 20 February 2019)

A d-dimensional second-order topological insulator (SOTI) can host topologically protected $(d-2)$-dimensional gapless boundary modes. Here, we show that a 2D non-Hermitian SOTI can host zero-energy modes at its corners. In contrast to the Hermitian case, these zero-energy modes can be localized only at one corner. A 3D non-Hermitian SOTI is shown to support second-order boundary modes, which are localized not along hinges but anomalously at a corner. The usual bulk-corner (hinge) correspondence in the second-order 2D (3D) non-Hermitian system breaks down. The winding number (Chern number) based on complex wave vectors is used to characterize the second-order topological phases in 2D (3D). A possible experimental situation with ultracold atoms is also discussed. Our work lays the cornerstone for exploring higher-order topological phenomena in non-Hermitian systems.

DOI: 10.1103/PhysRevLett.122.076801

Introduction.—Recent years have witnessed a surge of theoretical and experimental interest in studying topological phases [1–3] in insulators [4–9], superconductors [10–12], ultracold atoms [13–18], and classical waves [19–22]. These topologically nontrivial phases are characterized by the topological index of gapped bulk-energy bands and exhibit gapless states on their boundaries. Such gapless boundary states cannot be gapped out by local perturbations that preserve both bulk gap and symmetry.

Topological phases have widely been studied in closed systems, which are described by Hermitian Hamiltonians featuring real eigenenergies and orthogonal eigenstates. Recently, there has been a great deal of effort in exploring topological invariants of open systems governed by non-Hermitian operators [23,24]. Non-Hermitian Hamiltonians can find applications in a wide range of systems including optical and mechanical structures subjected to gain and loss [25–40], and solid-state systems with finite quasiparticle lifetimes [41–45]. In particular, topological phases of non-Hermitian Hamiltonians have recently been investigated in these systems [43–70]. The most prominent feature of non-Hermitian Hamiltonians is the existence of exceptional points (EPs), where more than one eigenstate coalesces [24,71,72]. This coalescence of eigenstates at EPs makes the corresponding eigenspace no longer complete, and the non-Hermitian Hamiltonian becomes nondiagonalizable. These unique features of EPs can lead to rich topological features in non-Hermitian topological systems with no counterpart in Hermitian cases such as Weyl exceptional rings [51], bulk Fermi arcs, and half-integer topological charges [57]. Furthermore, the interplay between non-Hermiticity and topology can lead to the breakdown of the usual bulk-boundary correspondence [50,52,58,63,65–67] due to the non-Bloch-wave behavior of open-boundary eigenstates, where the conventional Bloch wave functions do not precisely describe topological-phase transitions under the open-boundary conditions. The non-Bloch winding (Chern) number defined via complex wave vectors in 1D (2D) has recently been introduced to fill this gap [65,66].

More recently, the concept of topological insulators (TIs) has been generalized to second-order [73–91] and third-order [74,92,93] TIs in Hermitian systems. In contrast to conventional first-order TIs, a d-dimensional second-order topological insulator (SOTI) only hosts topologically protected $(d-2)$-dimensional gapless boundary states. For example, a 2D SOTI has zero-energy states localized at its corners, and a 3D SOTI hosts 1D gapless modes along its hinges. Therefore, the conventional bulk-boundary correspondence is no longer applicable to SOTIs. Up to now, studies of the second-order and third-order topological phases have been restricted to Hermitian systems. We now ask: is it possible for a non-Hermitian system to exhibit second-order topological phases? If yes, how can we define a topological invariant to characterize them?

In this Letter, we investigate 2D and 3D SOTIs described by non-Hermitian Hamiltonians. Even though the bulk bands are first-order topologically trivial insulators, there are degenerate second-order bound states. In contrast to the Hermitian case, these zero-energy states in 2D are localized only at one corner protected by mirror-rotation symmetry and sublattice symmetry. Moreover, the second-order boundary modes in 3D are localized not along the hinges but anomalously at a corner. The winding number (Chern number) characterizes its second-order topological phase in 2D (3D), where the non-Bloch-wave behavior of open-boundary eigenstates is included due to the breakdown of the usual bulk-corner (hinge) correspondence in second-order non-Hermitian systems. The proposed non-Hermitian model can experimentally be realized in ultracold atoms.

2D SOTI.—We consider a 2D non-Hermitian Hamiltonian H_{2D} that respects both twofold mirror-rotation symmetry $\mathcal{M}_{xy}$ and sublattice symmetry $\mathcal{S}$

$$\mathcal{M}_{xy}H_{2D}(k_x,k_y)\mathcal{M}_{xy}^{-1} = H_{2D}(k_y,k_x), \tag{1}$$

$$\mathcal{S}H(k_x,k_y)\mathcal{S}^{-1} = -H(k_x,k_y), \tag{2}$$

and $[\mathcal{S},\mathcal{M}_{xy}] = 0$. Note that the Hermitian counterpart with the same symmetries was investigated in Ref. [81]. Because of the mirror-rotation symmetry in Eq. (1), we can express the Hamiltonian H_{2D} on the high-symmetry line $k_x = k_y$ as

$$U^{-1}H_{2D}(k,k)U = \begin{pmatrix} H_+(k) & 0 \\ 0 & H_-(k) \end{pmatrix}, \tag{3}$$

where U is a unitary operator, and $H_\pm(k)$ acts on the mirror-rotation subspace. Since $H_\pm(k)$ respects sublattice symmetry $\mathcal{S}'$ defined in each mirror-rotation subspace [note that $\mathcal{S}$ in Eq. (2) is defined in the entire lattice space], we can define the winding number as follows:

$$w_\pm \coloneqq \oint_{\mathrm{BZ}} \frac{dk}{4\pi i}\mathrm{Tr}\left[\mathcal{S}'H_\pm^{-1}(k)\frac{dH_\pm(k)}{dk}\right]. \tag{4}$$

The topological index that characterizes the second-order topological phases in 2D is given by

$$w \coloneqq w_+ - w_-. \tag{5}$$

We investigate a concrete model of a 2D SOTI on a square lattice, where each unit cell contains four orbitals and asymmetric particle hopping within each unit cell is introduced, as shown in Fig. 1(a). The Bloch Hamiltonian is written as

$$\begin{aligned} H_{2D} = {}& [t+\lambda\cos(k_x)]\tau_x - [\lambda\sin(k_x)+i\gamma]\tau_y\sigma_z \\ & + [t+\lambda\cos(k_y)]\tau_y\sigma_y + [\lambda\sin(k_y)+i\gamma]\tau_y\sigma_x, \end{aligned} \tag{6}$$

where we have set the lattice constant $a_0 = 1$, λ is a real-valued intercell hopping amplitude, $t\pm\gamma$ denote real-valued asymmetric intracell hopping amplitudes, and σ_i and τ_i ($i = x,\, y,\, z$) are Pauli matrices for the degrees of freedom within a unit cell. The Hamiltonian H_{2D} can be implemented experimentally using ultracold atoms in optical lattices with engineered dissipation [see Fig. 1(b) and Sec. VIII in the Supplemental Material [94] for details]. The Hermitian part of $H_{2D}(\mathbf{k})$ preserves mirror and fourfold rotational symmetries with $\mathcal{M}_x = \tau_x\sigma_z$, $\mathcal{M}_y = \tau_x\sigma_x$, and $C_4 = [(\tau_x - i\tau_y)\sigma_0 - (\tau_x + i\tau_y)(i\sigma_y)]/2$. While they are broken by asymmetric hopping, H_{2D} stays invariant under sublattice symmetry $\mathcal{S} = \tau_z$ and mirror-rotation symmetry $\mathcal{M}_{xy} = C_4\mathcal{M}_y$, and $[\mathcal{S},\mathcal{M}_{xy}] = 0$.

Bulk and edge states.—The upper and lower bands $E_\pm(\mathbf{k})$ of $H(\mathbf{k})$ are twofold degenerate [94], and these bands coalesce at EPs with $E_\pm(\mathbf{k}_{\mathrm{EP}}) = 0$ for $t = \pm\lambda\pm\gamma$ or $\pm\sqrt{\gamma^2-\lambda^2}$. Figure 2 shows the complex energy spectra with open and periodic boundaries along the x and y directions, respectively. The non-Hermitian system supports gapped complex edge states for $|t| < |\gamma| + |\lambda|$, as shown in the red curves in Figs. 2(a) and 2(b). On the other hand, for $|t| > |\gamma| + |\lambda|$, there are no edge states [see Figs. 2(c) and 2(d)]. In spite of their existence, edge states can

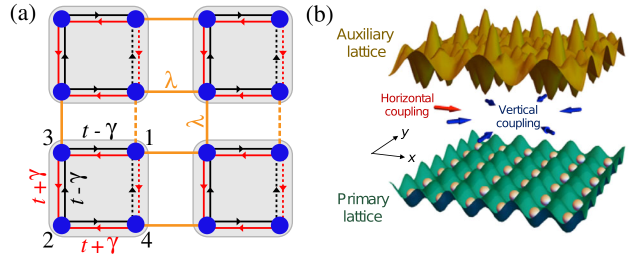

FIG. 1. Non-Hermitian SOTI in 2D. (a) Tight-binding representation of the model [Eq. (6)] on a square lattice. Each unit cell contains four orbitals (blue solid circles). The orange lines denote intercell coupling, and the red and black lines with arrows represent asymmetric intracell hopping. The dashed lines indicate hopping terms with a negative sign, accounting for a flux of π piercing each plaquette. (b) Schematic illustration of a proposed experimental setup using ultracold atoms [94]. The primary lattice together with a pair of Raman lasers gives rise to a Hermitian SOTI, where the Raman lasers are used for inducing effective particle hopping. The asymmetric hopping amplitudes are introduced via coherent coupling to a dissipative auxiliary lattice.

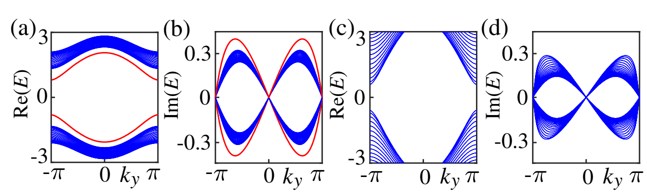

FIG. 2. Complex energy spectra of the non-Hermitian SOTI described by Eq. (6) with open boundaries along the x direction and periodic boundaries along the y direction. The edge states (red curves) are gapped for (a),(b) $t = 0.6$. No edge states exist for (c),(d) $t = 2.0$. An EP exists for $t = \lambda + \gamma = 1.9$, where a phase transition occurs. The number of unit cells along the x direction is $N = 20$ with $\lambda = 1.5$ and $\gamma = 0.4$.

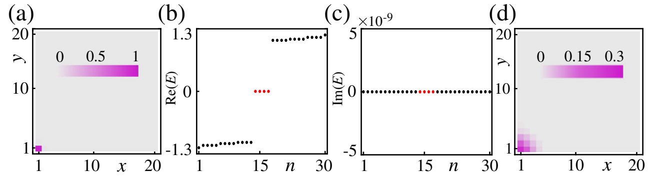

FIG. 3. Corner states in the non-Hermitian SOTI described by the Hamiltonian (6). (a) Probability density distributions $\sum_{i=1}^{4}|\phi_{R,i,n}|^2$ (n is the index of an eigenstate and R specifies a unit cell) of four zero-energy states under the open-boundary condition along the x and y directions. The zero-energy modes are localized only at the lower-left corner. (b),(c) Real and imaginary parts of complex eigenenergies around zero energy. The red dots represent eigenenergies of the corner modes. The imaginary parts of the bulk eigenenergies of a finite-size sample vanish over a wide range of parameters. (d) Probability density distribution of a typical bulk state under the open-boundary condition along the x and y directions. The bulk state is exponentially localized at the lower-left corner. The number of unit cells is 20×20 with $t = 0.6$, $\lambda = 1.5$, and $\gamma = 0.4$.

continuously be absorbed into bulk bands and therefore are not topologically protected. In fact, the bulk bands are topologically trivial, characterized by zero Chern number (see Sec. I in Ref. [94]) over the entire range of parameters.

Corner states.—While the bulk bands of $H(\mathbf{k})$ are topologically trivial, the system with open-boundary conditions in the x and y directions hosts four zero-energy modes at its corners, as shown in Figs. 3(a)–3(c). Moreover, these zero-energy states are localized only at the lower-left corner [see Fig. 3(a)]. Note that the midgap modes can be localized at the upper-right corner if the sign of hopping amplitude t is reversed (see Fig. S1 in Ref. [94]). This midgap-state localization at one corner results from the interplay between the symmetry $\mathcal{M}_{xy}$ and non-Hermiticity, where each corner mode is a simultaneously topological state of two intersecting nontrivial edges (see Sec. III in Ref. [94]). Furthermore, these corner modes are topologically protected against disorder preserving $\mathcal{M}_{xy}$ symmetry and sublattice symmetry (see Sec. IV in Ref. [94]). Note that when the mirror-rotation symmetry is broken, the midgap modes can be localized at more than one corner, and the sites at which mode localization occurs can be diagnosed by considering the type of asymmetric hopping and non-Hermiticity in non-Hermitian SOTIs (see Sec. V in Ref. [94]).

Moreover, the bulk bands of the *open*-boundary system are considerably different from those of the *periodic* system. As shown in Figs. 3(b) and 3(c), the bulk eigenenergies in the case of open boundaries are entirely real over a wide range of system parameters as a consequence of pseudo-Hermiticity of the open-boundary system [94], while they are complex in the case of the periodic boundaries. Furthermore, we find that, in contrast to the Hermitian SOTI, the bulk modes are exponentially localized at the lower-left corner due to the non-Hermiticity caused by the asymmetric hopping (see Sec. VI and VII in Ref. [94]), as shown in Fig. 3(d).

Topological index.—The topology of the non-Hermitian Hamiltonian H_{2D} is characterized by the winding number w [see Eqs. (1)–(5)]. One of the boundaries of the topological-phase transition calculated by this index is $t = \lambda + \gamma = 1.9$ (i.e., one of the EPs) using the parameters in Fig. 2. However, numerical calculations for the open-boundary system show that corner states exist only for $t < \sqrt{\lambda^2 + \gamma^2} \simeq 1.55$. Therefore, this topological index cannot correctly determine the phase boundary between topologically trivial and nontrivial regimes, indicating the breakdown of the usual bulk-corner correspondence in non-Hermitian systems. This breakdown results from the non-Bloch-wave behavior of open-boundary eigenstates of a non-Hermitian Hamiltonian, as studied in first-order topological insulators in Refs. [65,66]. To figure out this unexpected non-Bloch-wave behavior, *complex* wave vectors, instead of real ones, are suggested for defining the topological index of non-Hermitian systems [65,66]. Here, we generalize this idea to the non-Hermitian SOTI (see Sec. VII in Ref. [94] for details). After replacing real wave vectors $\mathbf{k}$ with complex ones

$$\mathbf{k} = (k_x, k_y) \to \tilde{\mathbf{k}} = (k_x - i\ln(\beta_0), k_y - i\ln(\beta_0)), \quad (7)$$

with $\beta_0 = \sqrt{|(t-\gamma)/(t+\gamma)|}$, the Hamiltonian $H_\pm$ for H_{2D} in Eq. (3) has the following forms:

$$\frac{\tilde{H}_\pm}{\sqrt{2}} = (t - \gamma + \lambda\beta_0 e^{ik})\sigma_\mp + \left(t + \gamma + \frac{\lambda}{\beta_0}e^{-ik}\right)\sigma_\pm, \quad (8)$$

where $\sigma_\pm = (\sigma_x \pm i\sigma_y)/2$. Note that the location of the midgap corner modes depends on β_0: they are localized at the lower-left corners for $\beta_0 < 1$, and at the upper-right corners for $\beta_0 > 1$. Figure 4(a) shows the topological-phase diagram. The number of zero-energy corner modes is counted as $2|w|$. Furthermore, the phase boundaries are determined by $t^2 = \lambda^2 + \gamma^2$ and $t^2 = \gamma^2 - \lambda^2$, and the phase

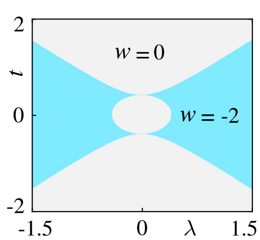

FIG. 4. Topological phase diagram in the 2D non-Hermitian SOTI for $\gamma = 0.4$. The gray regions represent the topologically trivial phase with $w = 0$, while the cyan regions represent the second-order topological phase with $w = -2$ that hosts corner states. The phase boundaries are determined by $t^2 = \lambda^2 + \gamma^2$ and $t^2 = \gamma^2 - \lambda^2$.

diagram contains the trivial phase ($w = 0$) and the second-order topological phase ($w = -2$).

3D SOTI.—We now consider a 3D non-Hermitian Hamiltonian H_{3D} that respects twofold mirror-rotation symmetry

$$\mathcal{M}_{xy} H_{3D}(k_x, k_y, k_z) \mathcal{M}_{xy}^{-1} = H_{3D}(k_y, k_x, k_z). \tag{9}$$

Note that the Hermitian counterpart was investigated in Ref. [82]. As in the 2D case, due to the mirror-rotation symmetry in Eq. (9), we can express the Hamiltonian H_{3D} along the high-symmetry line $k_x = k_y$ as

$$U^{-1} H_{3D}(k, k, k_z) U = \begin{pmatrix} H_+(k, k_z) & 0 \\ 0 & H_-(k, k_z) \end{pmatrix}, \tag{10}$$

where $H_\pm(k, k_z)$ acts on the corresponding mirror-rotation subspace. We can define the Chern number

$$C_\pm := \frac{1}{2\pi} \int_{\mathrm{BZ}} \mathrm{Tr}[dA_\pm + iA_\pm \wedge A_\pm], \tag{11}$$

where $A_\pm^{\alpha\beta} = i\langle \chi_\pm^\alpha(k, k_z) | d\phi_\pm^\beta(k, k_z) \rangle$ with α and β taken over the filled bands, and $|\phi_\pm^\alpha\rangle$ ($|\chi_\pm^\alpha\rangle$) is a right (left) eigenstate of $H_\pm(k, k_z)$. This formula is a natural generalization of the single-band non-Hermitian Chern number discussed in Ref. [53] to multiple bands. Then the topological index that characterizes the second-order topological phases in 3D is

$$C := C_+ - C_-. \tag{12}$$

We investigate a concrete model of a 3D non-Hermitian SOTI on a cubic lattice described by

$$H_{3D} = \left(m + t \sum_i \cos k_i \right) \tau_z + \sum_i (\Delta_1 \sin k_i + i\gamma_i) \sigma_i \tau_x + \Delta_2 (\cos k_x - \cos k_y) \tau_y, \tag{13}$$

where i runs over x, y, and z, and $\gamma_x = \gamma_y = \gamma_0$. This Hamiltonian H_{3D} only preserves mirror-rotation symmetry $\mathcal{M}_{xy}$ (see Sec. IX in Ref. [94]).

When the bulk bands of H_{3D} are gapped and first-order topologically trivial, it does not support gapless surface states, as shown by energy spectra with open boundaries along the y direction in Figs. 5(a) and 5(b). However, the system with open boundaries in both x and y directions hosts fourfold degenerate second-order boundary modes, as shown in Figs. 5(c) and 5(d). In contrast to the Hermitian case [82], these second-order boundary modes under the open-boundary condition along all the directions are localized not along the hinge but anomalously localized at one corner [see Fig. 5(e)]. This indicates that the usual bulk-hinge correspondence is broken for the 3D non-Hermitian SOTI. Moreover, these second-order boundary modes are only localized at the corners on the $x = y$ plane due to the mirror-rotation symmetry $\mathcal{M}_{xy}$ (see Fig. S10 in Ref. [94]). In addition, the second-order boundary modes can be localized at more than one corner when the mirror-rotation symmetry is broken or there exists the balanced gain and loss (see Sec. IX in Ref. [94]).

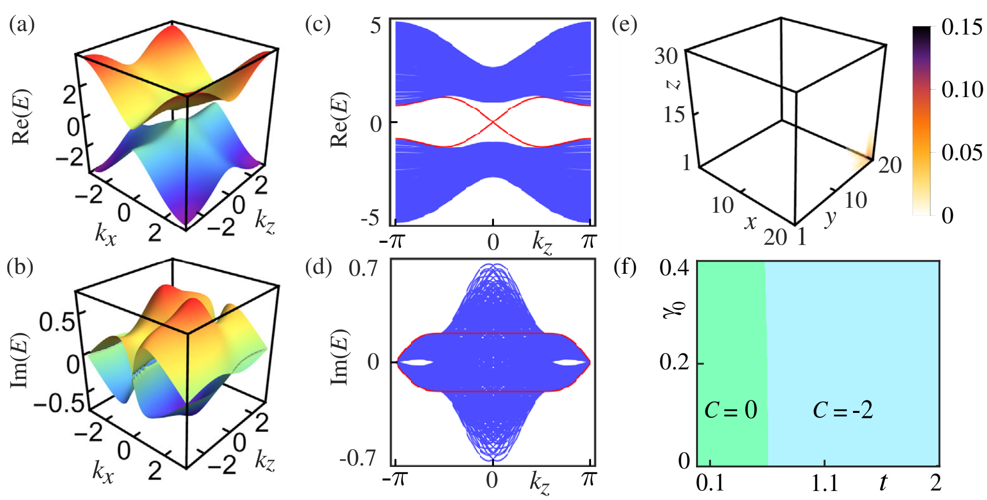

FIG. 5. Three-dimensional non-Hermitian SOTI described by Eq. (13). (a),(b) Complex energy spectrum under the open-boundary condition along the y direction. (c),(d) Complex energy spectrum under the open-boundary condition along the x and y directions. Red curves denote fourfold degenerate second-order boundary modes. (e) Probability density distribution $|\Phi_{n,R}|^2$ (n is the index of an eigenstate and R specifies a lattice site) of midgap modes with open boundaries along the x, y, and z directions. The midgap states (with eigenenergies of 0.035) are localized only at one corner. The number of unit cells is $20 \times 20 \times 30$ with $t = 1$, $\gamma_0 = 0.7$, $\gamma_z = -0.2$, $m = -2$, $\Delta_1 = 1.2$, and $\Delta_2 = 1.2$. (f) Second-order topological-phase diagram characterized by the nonzero Chern number.

Because of mirror-rotation symmetry, the second-order topological phase in 3D can be characterized by the Chern number C [see Eqs. (9)–(12)]. To generalize the bulk-boundary correspondence in 3D non-Hermitian SOTIs, we take into account the exponential-decay behavior of non-Hermitian eigenstates with open boundaries along all the directions. After considering a low-energy continuum model of the Hamiltonian H_{3D} to capture the essential physics of the 3D non-Hermitian SOTI with analytical results, and replacing real wave vectors $\mathbf{k}$ with complex ones (see Sec. IX in Ref. [94] for details), the Hamiltonian $H_\pm$ for H_{3D} in Eq. (10) can be expressed as

$$\begin{aligned}\bar{H}_\pm(k,k_z) = &-\left[m+3t-t(k-i\alpha_0)^2-\frac{t}{2}(k_z-i\alpha_z)^2\right]\sigma_z\\ &\pm\sqrt{2}[\Delta_1(k-i\alpha_0)+i\gamma_0]\sigma_y\\ &-\Delta_1(k_z-i\alpha_z)\sigma_x,\end{aligned}\tag{14}$$

where

$$\alpha_0=\frac{\gamma_0}{\Delta_1},\quad \text{and}\quad \alpha_z=\frac{\gamma_z}{\Delta_1}.\tag{15}$$

Figure 5(f) shows the topological-phase diagram, where the second-order topological phases are characterized by the nonzero Chern number ($C=-2$). The number of hinge states is counted as $2|C|$.

Conclusions.—In this Letter, we have analyzed 2D and 3D SOTIs in the presence of non-Hermiticity. In spite of their first-order topologically trivial bulk bands, second-order boundary modes exist in both 2D and 3D SOTIs. In contrast to the Hermitian cases, the midgap states in 2D are localized only at one corner protected by mirror-rotation symmetry and sublattice symmetry, and the second-order boundary modes are anomalously localized at a corner in 3D. The winding number (Chern number) defined by complex wave vectors is used to determine their second-order topological phases in 2D (3D). An experimental realization with ultracold atoms is also discussed. Our study provides a framework to explore richer non-Hermitian physics in higher-order topological phases.

T. L. thanks James Jun He for discussions, and Yi Peng for technical assistance. T. L. acknowledges support from a JSPS Postdoctoral Fellowship (P18023). Y. R. Z. was partially supported by China Postdoctoral Science Foundation (Grant No. 2018M640055). Z. G. was supported by MEXT. K. K. acknowledges support from the JSPS through the Program for Leading Graduate Schools (ALPS). M. U. acknowledges support by KAKENHI Grant No. JP18H01145 and a Grant-in-Aid for Scientific Research on Innovative Areas "Topological Materials Science (KAKENHI Grant No. JP15H05855) from the JSPS. F. N. is supported in part by the: MURI Center for Dynamic Magneto-Optics via the Air Force Office of Scientific Research (AFOSR) (Grant No. FA9550-14-1-0040), Army Research Office (ARO) (Grant No. W911NF-18-1-0358), Asian Office of Aerospace Research and Development (AOARD) (Grant No. FA2386-18-1-4045), Japan Science and Technology Agency (JST) (Q-LEAP program, ImPACT program, and CREST Grant No. JPMJCR1676), JSPS (JSPS-RFBR Grant No. 17-52-50023, and JSPS-FWO Grant No. VS.059.18N), RIKEN-AIST Challenge Research Fund, and the John Templeton Foundation.

Note added.—After this work was submitted, a related preprint [108] appeared, which focuses on the interplay between topological modes and skin boundary modes induced by nonreciprocity in non-Hermitian higher-order topological phases.

*tao.liu@riken.jp
†gong@cat.phys.s.u-tokyo.ac.jp
‡kawabata@cat.phys.s.u-tokyo.ac.jp
§ueda@phys.s.u-tokyo.ac.jp
‖fnori@riken.jp

[1] M. Z. Hasan and C. L. Kane, Colloquium: Topological insulators, Rev. Mod. Phys. **82**, 3045 (2010).
[2] X. L. Qi and S. C. Zhang, Topological insulators and superconductors, Rev. Mod. Phys. **83**, 1057 (2011).
[3] C. K. Chiu, J. C. Y. Teo, A. P. Schnyder, and S. Ryu, Classification of topological quantum matter with symmetries, Rev. Mod. Phys. **88**, 035005 (2016).
[4] F. D. M. Haldane, Model for a Quantum Hall Effect Without Landau Levels: Condensed-Matter Realization of the "Parity Anomaly", Phys. Rev. Lett. **61**, 2015 (1988).
[5] C. L. Kane and E. J. Mele, Z_2 Topological Order and the Quantum Spin Hall Effect, Phys. Rev. Lett. **95**, 146802 (2005).
[6] B. A. Bernevig, T. L. Hughes, and S. C. Zhang, Quantum spin Hall effect and topological phase transition in HgTe quantum wells, Science **314**, 1757 (2006).
[7] M. König, S. Wiedmann, C. Brüne, A. Roth, H. Buhmann, L. W. Molenkamp, X. L. Qi, and S. C. Zhang, Quantum spin Hall insulator state in HgTe quantum wells, Science **318**, 766 (2007).
[8] J. E. Moore and L. Balents, Topological invariants of time-reversal-invariant band structures, Phys. Rev. B **75**, 121306 (2007).
[9] H. Zhang, C. X. Liu, X. L. Qi, X. Dai, Z. Fang, and S. C. Zhang, Topological insulators in Bi_2Se_3, Bi_2Te_3 and Sb_2Te_3 with a single Dirac cone on the surface, Nat. Phys. **5**, 438 (2009).
[10] J. Alicea, New directions in the pursuit of Majorana fermions in solid state systems, Rep. Prog. Phys. **75**, 076501 (2012).
[11] C. W. J. Beenakker, Search for Majorana fermions in superconductors, Annu. Rev. Condens. Matter Phys. **4**, 113 (2013).
[12] M. Sato and Y. Ando, Topological superconductors: A review, Rep. Prog. Phys. **80**, 076501 (2017).
[13] M. Aidelsburger, M. Lohse, C. Schweizer, M. Atala, J. T. Barreiro, S. Nascimbène, N. R. Cooper, I. Bloch, and N. Goldman, Measuring the Chern number of

Hofstadter bands with ultracold bosonic atoms, Nat. Phys. **11**, 162 (2015).

[14] G. Jotzu, M. Messer, R. Desbuquois, M. Lebrat, T. Uehlinger, D. Greif, and T. Esslinger, Experimental realization of the topological Haldane model with ultracold fermions, Nature (London) **515**, 237 (2014).

[15] M. Lohse, C. Schweizer, O. Zilberberg, M. Aidelsburger, and I. Bloch, A Thouless quantum pump with ultracold bosonic atoms in an optical superlattice, Nat. Phys. **12**, 350 (2016).

[16] S. Nakajima, T. Tomita, S. Taie, T. Ichinose, H. Ozawa, L. Wang, M. Troyer, and Y. Takahashi, Topological Thouless pumping of ultracold fermions, Nat. Phys. **12**, 296 (2016).

[17] N. Goldman, J. C. Budich, and P. Zoller, Topological quantum matter with ultracold gases in optical lattices, Nat. Phys. **12**, 639 (2016).

[18] N. R. Cooper, J. Dalibard, and I. B. Spielman, Topological bands for ultracold atoms, arXiv:1803.00249 [Rev. Mod. Phys. (to be published)].

[19] A. B. Khanikaev, S. H. Mousavi, W. K. Tse, M. Kargarian, A. H. MacDonald, and G. Shvets, Photonic topological insulators, Nat. Mater. **12**, 233 (2013).

[20] L. Lu, J. D. Joannopoulos, and M. Soljačić, Topological photonics, Nat. Photon. **8**, 821 (2014).

[21] R. Süsstrunk and S. D. Huber, Observation of phononic helical edge states in a mechanical topological insulator, Science **349**, 47 (2015).

[22] A. B. Khanikaev and G. Shvets, Two-dimensional topological photonics, Nat. Photonics **11**, 763 (2017).

[23] C. M. Bender and S. Boettcher, Real Spectra in Non-Hermitian Hamiltonians Having $\mathcal{PT}$ Symmetry, Phys. Rev. Lett. **80**, 5243 (1998).

[24] C. M. Bender, Making sense of non-Hermitian Hamiltonians, Rep. Prog. Phys. **70**, 947 (2007).

[25] K. G. Makris, R. El-Ganainy, D. N. Christodoulides, and Z. H. Musslimani, Beam Dynamics in $\mathcal{PT}$ Symmetric Optical Lattices, Phys. Rev. Lett. **100**, 103904 (2008).

[26] Y. D. Chong, L. Ge, and A. D. Stone, $\mathcal{PT}$-Symmetry Breaking and Laser-Absorber Modes in Optical Scattering Systems, Phys. Rev. Lett. **106**, 093902 (2011).

[27] A. Regensburger, C. Bersch, M. A. Miri, G. Onishchukov, D. N. Christodoulides, and U. Peschel, Paritytime synthetic photonic lattices, Nature (London) **488**, 167 (2012).

[28] H. Jing, S. K. Özdemir, X. Y. Lü, J. Zhang, L. Yang, and F. Nori, $\mathcal{PT}$-Symmetric Phonon Laser, Phys. Rev. Lett. **113**, 053604 (2014).

[29] H. Hodaei, M. A. Miri, M. Heinrich, D. N. Christodoulides, and M. Khajavikhan, Parity-time–symmetric microring lasers, Science **346**, 975 (2014).

[30] B. Peng, Ş. K. Özdemir, F. Lei, F. Monifi, M. Gianfreda, G. L. Long, S. Fan, F. Nori, C. M. Bender, and L. Yang, Parity–time-symmetric whispering-gallery microcavities, Nat. Phys. **10**, 394 (2014).

[31] L. Feng, Z. J. Wong, R. M. Ma, Y. Wang, and X. Zhang, Single-mode laser by parity-time symmetry breaking, Science **346**, 972 (2014).

[32] B. Peng, Ş. K. Özdemir, S. Rotter, H. Yilmaz, M. Liertzer, F. Monifi, C. M. Bender, F. Nori, and L. Yang, Loss-induced suppression and revival of lasing, Science **346**, 328 (2014).

[33] H. Jing, Ş. K. Özdemir, Z. Geng, J. Zhang, X. Y. Lü, B. Peng, L. Yang, and F. Nori, Optomechanically-induced transparency in parity-time-symmetric microresonators, Sci. Rep. **5**, 9663 (2015).

[34] Z. P. Liu, J. Zhang, Ş. K. Özdemir, B. Peng, H. Jing, X. Y. Lü, C. W. Li, L. Yang, F. Nori, and Y. X. Liu, Metrology with $\mathcal{PT}$-Symmetric Cavities: Enhanced Sensitivity near the $\mathcal{PT}$-Phase Transition, Phys. Rev. Lett. **117**, 110802 (2016).

[35] K. Kawabata, Y. Ashida, and M. Ueda, Information Retrieval and Criticality in Parity-Time-Symmetric Systems, Phys. Rev. Lett. **119**, 190401 (2017).

[36] H. Jing, Ş. K. Özdemir, H. Lü, and F. Nori, High-order exceptional points in optomechanics, Sci. Rep. **7**, 3386 (2017).

[37] H. Lü, Ş. K. Özdemir, L. M. Kuang, F. Nori, and H. Jing, Exceptional Points in Random-Defect Phonon Lasers, Phys. Rev. Applied **8**, 044020 (2017).

[38] Y. Ashida, S. Furukawa, and M. Ueda, Parity-time-symmetric quantum critical phenomena, Nat. Commun. **8**, 15791 (2017).

[39] R. El-Ganainy, K. G. Makris, M. Khajavikhan, Z. H. Musslimani, S. Rotter, and D. N. Christodoulides, Non-Hermitian physics and PT symmetry, Nat. Phys. **14**, 11 (2018).

[40] J. Zhang, B. Peng, Ş. K. Özdemir, K. Pichler, D. O. Krimer, G. Zhao, F. Nori, Y. X. Liu, S. Rotter, and L. Yang, A phonon laser operating at an exceptional point, Nat. Photonics **12**, 479 (2018).

[41] H. Shen and L. Fu, Quantum Oscillation from In-Gap States and Non-Hermitian Landau Level Problem, Phys. Rev. Lett. **121**, 026403 (2018).

[42] A. A. Zyuzin and A. Yu. Zyuzin, Flat band in disorder-driven non-Hermitian Weyl semimetals, Phys. Rev. B **97**, 041203 (2018).

[43] M. Papaj, H. Isobe, and L. Fu, Nodal arc in disordered Dirac fermions: Connection to non-Hermitian band theory, arXiv:1802.00443.

[44] V. Kozii and L. Fu, Non-Hermitian topological theory of finite-lifetime quasiparticles: Prediction of bulk Fermi Arc due to exceptional point, arXiv:1708.05841.

[45] T. Yoshida, R. Peters, and N. Kawakami, Non-Hermitian perspective of the band structure in heavy-fermion systems, Phys. Rev. B **98**, 035141 (2018).

[46] M. S. Rudner and L. S. Levitov, Topological Transition in a Non-Hermitian Quantum Walk, Phys. Rev. Lett. **102**, 065703 (2009).

[47] K. Esaki, M. Sato, K. Hasebe, and M. Kohmoto, Edge states and topological phases in non-Hermitian systems, Phys. Rev. B **84**, 205128 (2011).

[48] S. Malzard, C. Poli, and H. Schomerus, Topologically Protected Defect States in Open Photonic Systems with Non-Hermitian Charge-Conjugation and Parity-Time Symmetry, Phys. Rev. Lett. **115**, 200402 (2015).

[49] S. Weimann, M. Kremer, Y. Plotnik, Y. Lumer, S. Nolte, K. G. Makris, M. Segev, M. C. Rechtsman, and A. Szameit, Topologically protected bound states in photonic paritytime-symmetric crystals, Nat. Mater. **16**, 433 (2017).

[50] T. E. Lee, Anomalous Edge State in a Non-Hermitian Lattice, Phys. Rev. Lett. **116**, 133903 (2016).

[51] Y. Xu, S. T. Wang, and L. M. Duan, Weyl Exceptional Rings in a Three-Dimensional Dissipative Cold Atomic Gas, Phys. Rev. Lett. **118**, 045701 (2017).
[52] D. Leykam, K. Y. Bliokh, C. Huang, Y. D. Chong, and F. Nori, Edge Modes, Degeneracies, and Topological Numbers in Non-Hermitian Systems, Phys. Rev. Lett. **118**, 040401 (2017).
[53] H. Shen, B. Zhen, and L. Fu, Topological Band Theory for Non-Hermitian Hamiltonians, Phys. Rev. Lett. **120**, 146402 (2018).
[54] V. M. Martinez Alvarez, J. E. Barrios Vargas, and L. E. F. Foa Torres, Non-Hermitian robust edge states in one dimension: Anomalous localization and eigenspace condensation at exceptional points, Phys. Rev. B **97**, 121401 (2018).
[55] G. Harari, M. A. Bandres, Y. Lumer, M. C. Rechtsman, Y. D. Chong, M. Khajavikhan, D. N. Christodoulides, and M. Segev, Topological insulator laser: Theory, Science **359**, eaar4003 (2018).
[56] M. A. Bandres, S. Wittek, G. Harari, M. Parto, J. Ren, M. Segev, D. N. Christodoulides, and M. Khajavikhan, Topological insulator laser: Experiments, Science **359**, eaar4005 (2018).
[57] H. Zhou, C. Peng, Y. Yoon, C. W. Hsu, K. A. Nelson, L. Fu, J. D. Joannopoulos, M. Soljačić, and B. Zhen, Observation of bulk Fermi arc and polarization half charge from paired exceptional points, Science **359**, 1009 (2018).
[58] X. Ye, Why does bulk boundary correspondence fail in some non-hermitian topological models, J. Phys. Commun. **2**, 035043 (2018).
[59] M. Pan, H. Zhao, P. Miao, S. Longhi, and L. Feng, Photonic zero mode in a non-hermitian photonic lattice, Nat. Commun. **9**, 1308 (2018).
[60] Z. Gong, Y. Ashida, K. Kawabata, K. Takasan, S. Higashikawa, and M. Ueda, Topological Phases of Non-Hermitian Systems, Phys. Rev. X **8**, 031079 (2018).
[61] Y. Chen and H. Zhai, Hall conductance of a non-Hermitian Chern insulator, Phys. Rev. B **98**, 245130 (2018).
[62] K. Kawabata, S. Higashikawa, Z. Gong, Y. Ashida, and M. Ueda, Topological unification of time-reversal and particle-hole symmetries in non-Hermitian physics, Nat. Commun. **10**, 297 (2019).
[63] F. K. Kunst, E. Edvardsson, J. C. Budich, and E. J. Bergholtz, Biorthogonal Bulk-Boundary Correspondence in Non-Hermitian Systems, Phys. Rev. Lett. **121**, 026808 (2018).
[64] K. Kawabata, Y. Ashida, H. Katsura, and M. Ueda, Parity-time-symmetric topological superconductor, Phys. Rev. B **98**, 085116 (2018).
[65] S. Yao and Z. Wang, Edge States and Topological Invariants of Non-Hermitian Systems, Phys. Rev. Lett. **121**, 086803 (2018).
[66] S. Yao, F. Song, and Z. Wang, Non-Hermitian Chern Bands, Phys. Rev. Lett. **121**, 136802 (2018).
[67] K. Kawabata, K. Shiozaki, and M. Ueda, Anomalous helical edge states in a non-Hermitian Chern insulator, Phys. Rev. B **98**, 165148 (2018).
[68] H. Wang, J. Ruan, and H. Zhang, Non-Hermitian nodal-line semimetals, arXiv:1808.06162.
[69] C. H. Lee and R. Thomale, Anatomy of skin modes and topology in non-Hermitian systems, arXiv:1809.02125.
[70] Y. K. Bliokh, D. Leykam, M. Lein, and F. Nori, Topological non-Hermitian origin of surface Maxwell waves, arXiv:1901.00346.
[71] M. V. Berry, Physics of nonhermitian degenerecies, Czech. J. Phys. **54**, 1039 (2004).
[72] W. Heiss, The physics of exceptional points, J. Phys. A **45**, 444016 (2012).
[73] F. Zhang, C. L. Kane, and E. J. Mele, Surface State Magnetization and Chiral Edge States on Topological Insulators, Phys. Rev. Lett. **110**, 046404 (2013).
[74] W. A. Benalcazar, B. A. Bernevig, and T. L. Hughes, Quantized electric multipole insulators, Science **357**, 61 (2017).
[75] W. A. Benalcazar, B. A. Bernevig, and T. L. Hughes, Electric multipole moments, topological multipole moment pumping, and chiral hinge states in crystalline insulators, Phys. Rev. B **96**, 245115 (2017).
[76] J. Langbehn, Y. Peng, L. Trifunovic, F. von Oppen, and P. W. Brouwer, Reflection-Symmetric Second-Order Topological Insulators and Superconductors, Phys. Rev. Lett. **119**, 246401 (2017).
[77] F. K. Kunst, G. van Miert, and E. J. Bergholtz, Lattice models with exactly solvable topological hinge and corner states, Phys. Rev. B **97**, 241405 (2018).
[78] C. W. Peterson, W. A. Benalcazar, T. L. Hughes, and G. Bahl, A quantized microwave quadrupole insulator with topologically protected corner states, Nature (London) **555**, 346 (2018).
[79] M. Serra-Garcia, V. Peri, R. Süsstrunk, O. R. Bilal, T. Larsen, L. G. Villanueva, and S. D. Huber, Observation of a phononic quadrupole topological insulator, Nature (London) **555**, 342 (2018).
[80] Z. Song, Z. Fang, and C. Fang, $(d-2)$-Dimensional Edge States of Rotation Symmetry Protected Topological States, Phys. Rev. Lett. **119**, 246402 (2017).
[81] S. Imhof, C. Berger, F. Bayer, J. Brehm, L. W. Molenkamp, T. Kiessling, F. Schindler, C. H. Lee, M. Greiter, T. Neupert, and R. Thomale, Topolectrical-circuit realization of topological corner modes, Nat. Phys. **14**, 925 (2018).
[82] F. Schindler, A. M. Cook, M. G. Vergniory, Z. Wang, S. S. P. Parkin, B. A. Bernevig, and T. Neupert, Higher-order topological insulators, Sci. Adv. **4**, eaat0346 (2018).
[83] M. Ezawa, Magnetic second-order topological insulators and semimetals, Phys. Rev. B **97**, 155305 (2018).
[84] F. Schindler, Z. Wang, M. G. Vergniory, A. M. Cook, A. Murani, S. Sengupta, A. Y. Kasumov, R. Deblock, S. J. I. Drozdov, H. Bouchiat, S. Guron, A. Yazdani, B. A. Bernevig, and T. Neupert, Higher-order topology in Bismuth, Nat. Phys. **14**, 918 (2018).
[85] X. Zhu, TunableMajorana corner states in a two-dimensional second-order topological superconductor induced by magnetic fields, Phys. Rev. B **97**, 205134 (2018).
[86] J. Noh, W. A. Benalcazar, S. Huang, M. J. Collins, K. P. Chen, T. L. Hughes, and M. C. Rechtsman, Topological protection of photonic mid-gap defect modes, Nat. Photonics **12**, 408 (2018).

[87] M. Geier, L. Trifunovic, M. Hoskam, and P. W. Brouwer, Second-order topological insulators and superconductors with an order-two crystalline symmetry, Phys. Rev. B **97**, 205135 (2018).

[88] Z. Yan, F. Song, and Z. Wang, Majorana Corner Modes in a High-Temperature Platform, Phys. Rev. Lett. **121**, 096803 (2018).

[89] Q. Wang, C. C. Liu, Y. M. Lu, and F. Zhang, High-Temperature Majorana Corner States, Phys. Rev. Lett. **121**, 186801 (2018).

[90] T. Liu, J. J. He, and F. Nori, Majorana corner states in a two-dimensional magnetic topological insulator on a high-temperature superconductor, Phys. Rev. B **98**, 245413 (2018).

[91] A. Matsugatani and H. Watanabe, Connecting higher-order topological insulators to lower-dimensional topological insulators, Phys. Rev. B **98**, 205129 (2018).

[92] M. Ezawa, Higher-Order Topological Insulators and Semimetals on the Breathing Kagome and Pyrochlore Lattices, Phys. Rev. Lett. **120**, 026801 (2018).

[93] E. Khalaf, Higher-order topological insulators and superconductors protected by inversion symmetry, Phys. Rev. B **97**, 205136 (2018).

[94] See Supplemental Material at http://link.aps.org/supplemental/10.1103/PhysRevLett.122.076801 for (I) tight-binding Hamiltonian, (II) pseudo-Hermiticity, (III) edge theory, (IV) robustness against disorder, (V) effect of a different type of asymmetric hopping and non-Hermiticity on the localization of corner modes, (VI) degenerate perturbation theory, (VII) bulk-state localization and winding number, (VIII) possible experimental realization, and (IX) non-hermitian second-order topological phases in 3D, which includes Refs. [95–107].

[95] A. Mostafazadeh and Pseudo-, Hermiticity versus PT symmetry: The necessary condition for the reality of the spectrum of a non-Hermitian Hamiltonian, J. Math. Phys. (N.Y.) **43**, 205 (2002).

[96] A. Mostafazadeh, Pseudo-Hermiticity versus PT-symmetry. II. A complete characterization of non-Hermitian Hamiltonians with a real spectrum, J. Math. Phys. (N.Y.) **43**, 2814 (2002).

[97] A. Mostafazadeh, Pseudo-Hermiticity versus PT-symmetry. III. Equivalence of pseudo-Hermiticity and the presence of antilinear symmetries, J. Math. Phys. (N.Y.) **43**, 3944 (2002).

[98] J. J. Sakurai and J. Napolitano, *Modern Quantum Mechanics* (Addison-Wesley, Boston, 2011).

[99] P. Cappellaro, *Quantum Theory of Radiation Interactions* (MIT OpenCourseWare, Cambridge, Massachusetts, 2012).

[100] M. Mller, S. Diehl, G. Pupillo, and P. Zoller, Engineered open systems and quantum simulations with atoms and ions, Adv. At. Mol. Opt. Phys. **61**, 1 (2012).

[101] N. Goldman, G. Juzelinas, P. hberg, and I. B. Spielman, Light-induced gauge fields for ultracold atoms, Rep. Prog. Phys. **77**, 126401 (2014).

[102] M. Aidelsburger, M. Atala, M. Lohse, J. T. Barreiro, B. Paredes, and I. Bloch, Realization of the Hofstadter Hamiltonian with Ultracold Atoms in Optical Lattices, Phys. Rev. Lett. **111**, 185301 (2013).

[103] H. Miyake, G. A. Siviloglou, C. J. Kennedy, W. C. Burton, and W. Ketterle, Realizing the Harper Hamiltonian with Laser-Assisted Tunneling in Optical Lattices, Phys. Rev. Lett. **111**, 185302 (2013).

[104] A. L. Gaunt, T. F. Schmidutz, I. Gotlibovych, R. P. Smith, and Z. Hadzibabic, Bose-Einstein Condensation of Atoms in a Uniform Potential, Phys. Rev. Lett. **110**, 200406 (2013).

[105] F. Reiter and A. S. Sørensen, Effective operator formalism for open quantum systems, Phys. Rev. A **85**, 032111 (2012).

[106] T. D. Lee and C. N. Yang, Statistical theory of equations of state and phase transitions. II. Lattice gas and Ising model, Phys. Rev. **87**, 410 (1952).

[107] R. Jackiw and C. Rebbi, Solitons with fermion number $1/2$, Phys. Rev. D **13**, 3398 (1976).

[108] C. H. Lee, L. Li, and J. Gong, Hybrid higher-order skin-topological modes in non-reciprocal systems, arXiv:1810.11824.